Available online at www.sciencedirect.com

ScienceDirect

MATTER AND RADIATION AT EXTREMES

Matter and Radiation at Extremes 2 (2017) 3−8

www.journals.elsevier.com/matter-and-radiation-at-extremes

Letter

Non-equilibrium between ions and electrons inside hot spots from National Ignition Facility experiments

Zhengfeng Fan [a], Yuanyuan Liu [a], Bin Liu [a], Chengxin Yu [a,*], Ke Lan [a], Jie Liu [a,b]

[a] *Institute of Applied Physics and Computational Mathematics, Beijing 100088, China*
[b] *Center for Applied Physics and Technology, Peking University, Beijing 100871, China*

Received 22 August 2016; revised 5 November 2016; accepted 10 November 2016
Available online 18 December 2016

Abstract

The non-equilibrium between ions and electrons in the hot spot can relax the ignition conditions in inertial confinement fusion [Fan et al., Phys. Plasmas 23, 010703 (2016)], and obvious ion-electron non-equilibrium could be observed by our simulations of high-foot implosions when the ion-electron relaxation is enlarged by a factor of 2. On the other hand, in many shots of high-foot implosions on the National Ignition Facility, the observed X-ray enhancement factors due to ablator mixing into the hot spot are less than unity assuming electrons and ions have the same temperature [Meezan et al., Phys. Plasmas 22, 062703 (2015)], which is not self-consistent because it can lead to negative ablator mixing into the hot spot. Actually, this non-consistency implies ion-electron non-equilibrium within the hot spot. From our study, we can infer that ion-electron non-equilibrium exists in high-foot implosions and the ion temperature could be ~9% larger than the equilibrium temperature in some NIF shots.

PACS Codes: 52.57.-z; 52.30.-q

Keywords: Ion-electron non-equilibrium; Hot-spot ignition conditions relaxation; High-foot experiments

Hot-spot physics is important for ignition target design in inertial confinement fusion (ICF). Fusion reactions of deuterium and tritium (DT) within the hot spot take place at several keV to overcome the Coulomb barrier between fusing nuclei, and the hot spot needs to have sufficient areal density to enter a self-heating regime. In the laser-driven central hot-spot ignition [1−3], a spherical shell of cryogenic D-T fuel, coated with a low-Z ablator, is imploded nearly isentropically either directly by lasers or indirectly by X-ray radiation converted from laser beams to a high velocity, so that the fuel is highly compressed under the spherical convergent effect, and an ignition hot spot with an areal density of ~0.3 g/cm^2 and a temperature of ~5−10 keV is formed in the center, triggering a burn of the main fuel and resulting in a significant thermonuclear energy gain. Within the hot spot, it is commonly assumed that ions and electrons are in equilibrium. This assumption restricts the target optimizations in design and may lead to non-consistency in the experimental diagnostics as well.

Fan et al. have proposed an ion-electron non-equilibrium model for relaxing the central hot-spot ignition conditions [4]. In this model, the ions and electrons are assumed to have separate temperatures, i.e. T_i and T_e, and T_i is higher than T_e. Within the hot spot, fusion reaction is proportional to T_i^α with $\alpha \approx 2-3$, therefore a higher ion temperature can obviously enhance the hot-spot nuclear reactions. On the other side, the hot-spot energy leaks due to electron thermal conduction and

* Corresponding author.
E-mail address: cx_yu2013@163.com (C.X. Yu).

Peer review under responsibility of Science and Technology Information Center, China Academy of Engineering Physics.

http://dx.doi.org/10.1016/j.mre.2016.11.003

electron bremsstrahlung are proportional to $T_e^{7/2}$ and $T_e^{1/2}$, respectively. Therefore a lower electron temperature remarkably reduces the hot-spot energy leaks. The above two effects result in an enlarged ignition region in the hot-spot ρR–T space. According to the theory in Ref. [4], when the ion temperature becomes 10% higher than the equilibrium temperature, the required hot-spot ρR would reduce from ~0.32 g/cm^2 to ~0.17 g/cm^2 at a fixed equilibrium temperature of 5 keV. In this letter, we point out that obvious ion-electron non-equilibrium exits in ignition-scale capsule implosions and it can be observed in the National Ignition Facility (NIF) high-foot experiments. We will firstly discuss the thermal equilibration between ions and electrons, and then show the non-equilibrium phenomenon via simulation of an ignition-scale capsule implosion, and finally give an analysis of ion-electron non-equilibrium in the NIF high-foot experiments.

When ions and electrons have separate temperatures T_i and T_e, their thermal equilibration rate becomes important. For DT plasmas, the ion-electron energy inter-exchange via collisions is normally described by

$$\frac{dT_i}{dt} = -\frac{T_i - T_e}{\tau}, \tag{1}$$

$$\frac{dT_e}{dt} = \frac{T_i - T_e}{\tau}, \tag{2}$$

where τ is the relaxation time between ions and electrons. For a non-degenerate (ideal) plasma, the electrons have Maxwellian distribution [5],

$$\tau_{ideal} = 100\frac{T_e^{3/2}}{\rho \ln\Lambda}, \tag{3}$$

where τ_{ideal} and T_e are in units of ps and keV, respectively; the plasma density ρ is in the unit of g/cm^3; and $\ln\Lambda$ is the Coulomb logarithm. In ICF, the DT plasma is highly compressed and the electrons have Fermi–Dirac distribution which makes the ion-electron relaxation time longer than the non-degenerate case. In this case [5],

$$\tau = \tau_{ideal}\frac{2[1+\exp(-\mu/kT_e)]F_{1/2}(\mu/kT_e)}{\sqrt{\pi}}, \tag{4}$$

where μ is the chemical potential and $F_{1/2}(\mu/kT_e)$ is Fermi–Dirac integral. Fig. 1 shows the ion-electron relaxation time for densities ranging from 1 to 50 g/cm^3 and temperatures from 1 to 10 keV. We see that the ion-electron relaxation time is of tens of picoseconds when the temperature is >5 keV. In ICF, the deceleration phase of an ignition-scale capsule implosion lasts ~200–300 ps, and is ~100 ps since the capsule center has a density >10 g/cm^3. This implies that the ion-electron relaxation time within an ignition-scale hot spot is comparable to the deceleration phase, which creates preconditions for a non-equilibrium hot spot.

To study the non-equilibrium phenomenon, we considered a typical capsule used in the NIF [6] and its implosion dynamics was performed by our LARED-S code. The capsule

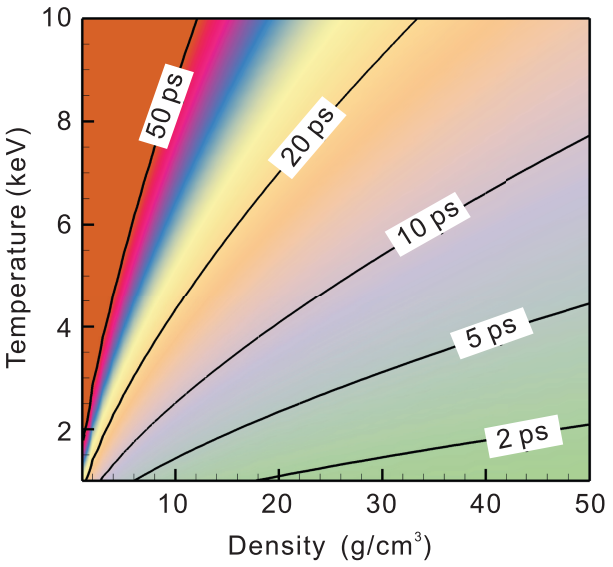

Fig. 1. Ion-electron relaxation time for different densities and temperatures.

cross-section is shown in Fig. 2(a). The CH ablator is 195 μm thick, and the DT ice is 69 μm thick. A high-foot radiation drive is shown in Fig. 2(b). A well tuned radiation temperature is plotted by red solid line, which has three steps, with an

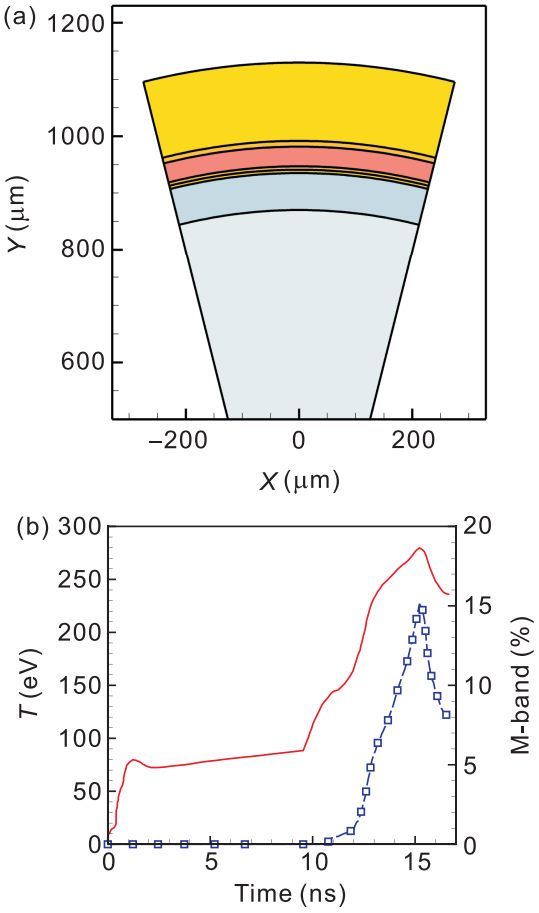

Fig. 2. (a) Sketch of the ignition capsule, (b) radiation drive pulse (red solid line) and M-band fraction (blue dashed line with hollow squares).

80 eV foot and a 280 eV peak. M-band (i.e. $h\nu > 1.8$ keV) was considered in our simulation, and the M-band was obtained by interpolation of the experimental data as given in Ref. [7]. The M-band fraction is plotted by blue dashed line with squares. Simulations of implosion dynamics of the capsules were performed by the radiation-hydrodynamics code LARED-S [8], which is multi-dimensional, massively parallel and Eulerian mesh based. Current simulations include multi-group radiation diffusion (30 groups), plasma hydrodynamics, electron thermal conductions, nuclear reaction, alpha particle transport, and the quotidian equations of state [9]. We emphasize that the ions and electrons are assumed to have separate temperatures in this simulation, and the ion-electron relaxation time is enlarged by a factor of 2 for the following reasons. Firstly, high energetic ions which contribute more to fusion reactions are less prone to equilibrate with electrons than low energetic ions; secondly, potential screening tends to increase the relaxation time between ions and electrons [10]. Specially, the energy equations for the ions and electrons are written as

$$\frac{\partial \rho e(\rho, T_\mathrm{i})}{\partial t} + \nabla\cdot[\rho e(\rho, T_\mathrm{i})\boldsymbol{V}] + p_\mathrm{i}\nabla\cdot\boldsymbol{V} = \nabla\cdot(-q_\mathrm{i}) - \omega_\mathrm{ei}(T_\mathrm{i} - T_\mathrm{e}) + W_{\alpha,\mathrm{i}}, \tag{5}$$

and

$$\frac{\partial \rho e(\rho, T_\mathrm{e})}{\partial t} + \nabla\cdot[\rho e(\rho, T_\mathrm{e})\boldsymbol{V}] + p_\mathrm{e}\nabla\cdot\boldsymbol{V} = \nabla\cdot(-q_\mathrm{e}) + \omega_\mathrm{ei}(T_\mathrm{i} - T_\mathrm{e}) + W_\mathrm{r} + W_{\alpha,\mathrm{e}}, \tag{6}$$

where $e(\rho,T_\mathrm{i})$ and $e(\rho,T_\mathrm{e})$ are the specific energies for ions and electrons, respectively; p_i and p_e are the pressures for ions and electrons, respectively; $\boldsymbol{V}$ is the velocity; q_i and q_e are the ion- and electron-thermal conductions, respectively; $\omega_\mathrm{ei}(T_\mathrm{i}-T_\mathrm{e})$ is the energy-exchange between ions and electrons; W_r is the energy-exchange between electrons and radiation; and, $W_{\alpha,\mathrm{i}}$ and $W_{\alpha,\mathrm{e}}$ are the thermonuclear alpha-particle energy deposition to ions and electrons, respectively.

Initially, the ion- and electron-temperatures are the same at the triple point of DT. As shocks pass through, the post-shock ion temperature gets higher than the electron temperature. Thereafter, the ion- and electron-temperatures get into equilibrium soon in the high-density low-temperature main-fuel region. Nevertheless, in the hot-spot region where the density is much lower and the temperature is much higher, observable ion-electron non-equilibrium exists before capsule stagnation.

Presented in Fig. 3 is the shock trajectories within the target. As shown, each step of the radiation drive launches an inward shock, with the first two shocks merging at the vicinity of the DT-ice inner surface, and the third one catching up with the former shock(s) within the DT gas, forming a much stronger one. As the strong shock propagates within the DT gas, it will distribute thermal energy among ions and electrons according to their masses. Due to the fact that the electron mass is thousands of times smaller than the ion mass of D or T, the immediate post-shock electron temperature is only a few times of the pre-shock

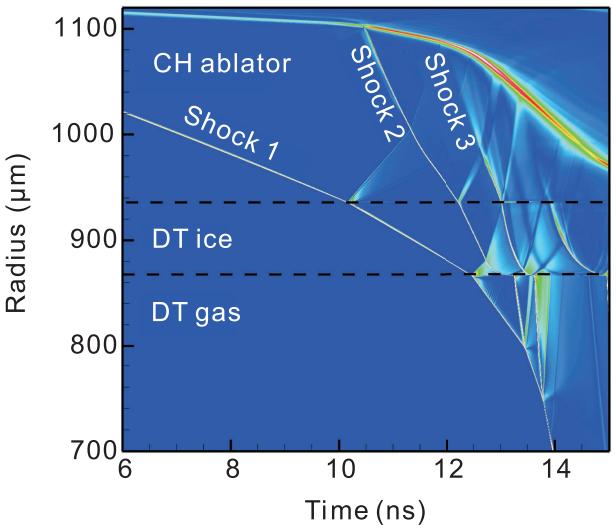

Fig. 3. Shock trajectories within the target.

electron temperature and remains low, and the immediate post-shock ion temperature increases suddenly as

$$T_{0\mathrm{i}} \approx \frac{3}{16} m_\mathrm{i} u_\mathrm{s}^2, \tag{7}$$

where m_i is the ion mass and u_s is the shock speed [11]. Thereafter, the relaxation between ions and electrons makes their temperatures become closer. Apart from that, thermonuclear alpha particles deposit more energy into electrons than into ions when the temperature is <32 keV [12], which also makes the ion- and electron-temperatures closer. Even though, the relaxation process needs a time, and the non-equilibrium lasts for a certain time period within the hot spot. Fig. 4(a)–(d) show the temperature and density profiles at 16.20 ns (time of peak implosion velocity), 16.30 ns, 16.40 ns and 16.47 ns (time of stagnation). At the time of peak implosion velocity, the ion temperature in the hot-spot center is ~7.5 keV, which is more than twice larger than its electron temperature of ~2.3 keV. At the time of stagnation, the ion temperature in the hot-spot center is ~10.0 keV, which is 20% larger than its electron temperature of ~8.5 keV. Fig. 5(a) and (b) show the histories of the hot-spot ion- and electron-temperatures in the space-time coordinate, respectively, while Fig. 4(e) shows the hot-spot average ion- and electron-temperatures [13]. And it is seen that the hot-spot ion temperature is obviously larger than its electron temperature, especially before the time of stagnation (i.e. 16.47 ns).

In fact, the non-equilibrium phenomena between T_i and T_e can be inferred from the experimental diagnostics of the high-foot implosion experiments conducted on NIF. Here, we present an evidence from the ablator-to-hot-spot mix level measurement experiments where the mix level is determined by the ratio of X-ray emission to the total neutron yield [14].

The X-ray emission from the hot spot can be written as

$$X_\nu = 4\pi \times j_\mathrm{DT} \times f_\mathrm{en} \times \exp\left(-\tau_\nu^\mathrm{shell}\right) \times V \times \Delta t, \tag{8}$$

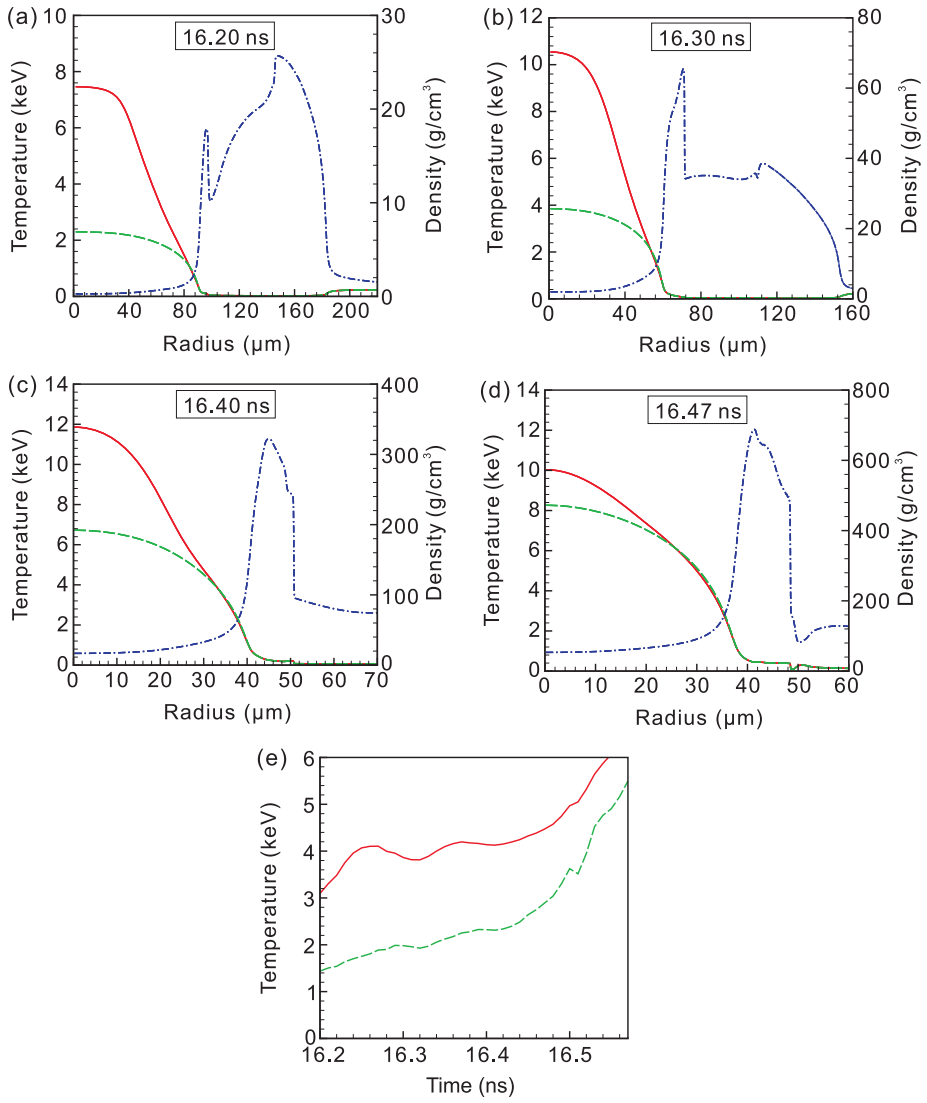

Fig. 4. Profiles of the ion and electron temperatures at (a) 16.20 ns, (b) 16.30 ns, (c) 16.40 ns and (d) 16.47 ns, respectively, and (e) history of the hot-spot average ion and electron temperatures. In (a)–(e), red solid lines plot the ion temperature, green dashed lines plot the electron temperature, and blue dash-dot lines plot the density.

where $j_{\rm DT} = 4n_{\rm D}n_{\rm T}\exp(-h\nu/kT_{\rm e})/A_\nu^2/h\nu^{0.33}$ is the total DT emissivity, with $n_{\rm D}$ and $n_{\rm T}$ being the number densities of deuterium and tritium ions, $h\nu$ the photon energy and A_ν the Avogadro's number; $\tau_\nu^{\rm shell}$ is the optical depth of the shell; V is the hot spot volume; and Δt is the burn duration. Especially,

$$f_{\rm en} = \left(1 + \sum x_i Z_i\right)\left(1 + \sum x_i \frac{j_i}{j_{\rm DT}}\right), \tag{9}$$

which represents the enhancement in emission due to mix of ions with atomic number Z_i, and fraction x_i of the total number of DT atoms. The total neutron yield $Y_{\rm DT}$ from D + T reaction is given by

$$Y_{\rm DT} = n_{\rm D} \times n_{\rm T} \times \langle \sigma v(T_{\rm i})\rangle \times V \times \Delta t, \tag{10}$$

where $\langle \sigma v(T_{\rm i})\rangle$ is the DT reactivity with ion temperature $T_{\rm i}$. Then, the ratio of X-ray emission to the total neutron yield could be written as

$$\frac{X_\nu}{Y_{\rm DT}} = \frac{16\pi\exp(-h\nu/kT_{\rm e})}{A_\nu^2(h\nu)^{0.33}\langle \sigma_{\rm DT} v(T_{\rm i})\rangle} \times f_{\rm en} \times \exp\left(-\tau_\nu^{\rm shell}\right). \tag{11}$$

Details for experimental measurements of the neutron yield $Y_{\rm DT}$, the ion temperature $T_{\rm i}$, the hot spot volume V, the burn duration Δt, etc. can be found in Refs. [14–20].

We emphasize that the assumption of $T_{\rm e} = T_{\rm i}$ makes the measured X-ray enhancement $f_{\rm en,m}$ deviate from the actual value $f_{\rm en}$ by a factor of $F_f = f_{\rm en}/f_{\rm en,m} = \exp[h\nu(T_{\rm i}-T_{\rm e})/(kT_{\rm i}T_{\rm e})]$. There may be no significant influence for a large level of ablator mix into the hot spot or an equilibrium hot spot. However, for NIF high-foot high-adiabat implosion experiments, the ablator mix into the hot spot is significantly suppressed, and the usage of $T_{\rm e} = T_{\rm i}$ leads to a result that is not self-consistent. According to the definition of the X-ray enhancement, $f_{\rm en}$ should be larger than unity, while nearly half of the high-foot shots have $f_{\rm en,m}$ less than unity in Ref. [21]. This inconsistency is caused by ion-electron non-equilibrium within the hot spot where the ion temperature is greater than the electron temperature. With the consideration of

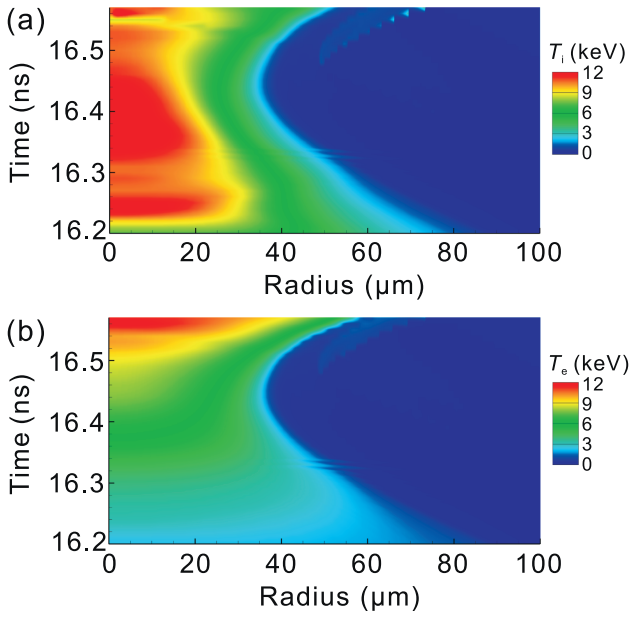

Fig. 5. Histories of (a) the ion temperature and (b) electron temperature in the space-time coordinate.

ion-electron non-equilibrium, the measured X-ray enhancement $f_{\mathrm{en,m}}$ could be written as

$$f_{\mathrm{en,m}} = \left(1+\sum x_i Z_i\right)\left(1+\sum x_i \frac{j_i}{j_{\mathrm{DT}}}\right) \times \exp[-h\nu(T_{\mathrm{i}}-T_{\mathrm{e}})/(kT_{\mathrm{i}}T_{\mathrm{e}})]. \tag{12}$$

The first term on the right hand side of Eq. (12) represents X-ray enhancement due to ablator mix, while the second term actually represents X-ray reduction due to ion-electron non-equilibrium. When ablator mix is dominant, $f_{\mathrm{en,m}}$ would be larger than unity. On the other hand, when ion-electron non-equilibrium is dominant, $f_{\mathrm{en,m}}$ would be less than unity. Assuming a nearly "clean" DT hot spot for the shots with $f_{\mathrm{en,m}}$ less than unity, we have

$$F_f \geq \frac{1}{f_{\mathrm{en,m}}}, \tag{13}$$

and

$$T_{\mathrm{e}} = \frac{h\nu T_{\mathrm{i}}}{h\nu + kT_{\mathrm{i}}\ln(F_f)} \leq \frac{h\nu T_{\mathrm{i}}}{h\nu - kT_{\mathrm{i}}\ln(f_{\mathrm{en,m}})}. \tag{14}$$

According to Eq. (14), we see that the electron temperature is actually less than the ion temperature when the measured X-ray enhancement factor is less than unity. To quantify the level of non-equilibrium within the hot spot, we define a non-equilibrium factor as

$$f = \frac{T_{\mathrm{i}}}{(T_{\mathrm{i}}+T_{\mathrm{e}})/2} \geq \frac{2h\nu - 2kT_i\ln(f_{\mathrm{en,m}})}{2h\nu - kT_i\ln(f_{\mathrm{en,m}})}. \tag{15}$$

Table 1
Non-equilibrium factors in some of NIF high-foot experiments.

Shot number	T_{i} (keV)	$f_{\mathrm{en,m}}$	f
N131119	5.0 ± 0.2	0.86 ± 0.18	$\geq 1.03 \pm 0.05$
N140120	5.1 ± 0.2	0.78 ± 0.16	$\geq 1.06 \pm 0.05$
N140225	4.5 ± 0.2	0.77 ± 0.16	$\geq 1.05 \pm 0.04$
N140707	4.7 ± 0.1	0.66 ± 0.14	$\geq 1.09 \pm 0.04$

Table 1 shows the non-equilibrium factors in some of NIF high-foot experiments. In this table, the uncertainty of the non-equilibrium factor is determined by $\Delta f = |\partial f/\partial T_{\mathrm{i}}| \cdot \Delta T_{\mathrm{i}} + |\partial f/\partial f_{\mathrm{en,m}}| \cdot \Delta f_{\mathrm{en,m}}$. We see that the hot spot have observable ion-electron non-equilibrium for these four shots with a maximum non-equilibrium factor of ~1.09.

In summary, both simulations of a high-foot ignition target (with a slightly enlarged ion-electron relaxation time) and analysis of the NIF high-foot diagnostics data support the existence of ion-electron non-equilibrium in the hot spot of high-foot implosions, and it is inferred that the ion temperature can be ~9% larger than the ion-electron equilibrium temperature in the high-foot experiments on NIF. This is an important observation because ion-electron non-equilibrium could enlarge the ignition region in the hot-spot $\rho R - T$ space [4], and a wedged-peak pulse can be utilized to create and maintain non-equilibrium conditions within the hot spot, reducing the hot-spot ρR requirement for achieving self-heating [22,4]. The existence evidence of hot-spot ion-electron non-equilibrium implies a new way for optimizing our ignition target design in inertial confinement fusion. In the near future, experiments will be done on the SG-III laser facility to show the benefits of optimizing the hot-spot non-equilibrium.

Acknowledgement

This work has been supported by the Foundation of President of China Academy of Engineering Physics (Grant Nos. 201402037 and 201401040), the CAEP-FESTC (Grant No. R2014-0501-01) and the National Basic Research Program of China (Grant No. 2013CB34100).

References

[1] J.H. Nuckolls, L. Wood, A. Thiessen, G.B. Zimmerman, Laser compression of matter to super-high densities: Thermonuclear (CTR) applications, Nature 239 (1972) 139.
[2] J.D. Lindl, Inertial Confinement Fusion, Springer, New York, 1998.
[3] S. Atzeni, J. Meyer-ter-Vehn, The Physics of Inertial Fusion, Clarendon Press, Oxford, 2004.
[4] Z.F. Fan, J. Liu, B. Liu, C.X. Yu, X.T. He, Ignition conditions relaxation for central hot-spot ignition with an ion-electron nonequilibrium model, Phys. Plasmas 23 (2016) 010703.
[5] Y.T. Lee, R.M. More, An electron conductivity model for dense plasmas, Phys. Fluids 27 (1984) 1273.
[6] T.R. Dittrich, O.A. Hurricane, D.A. Callahan, E.L. Dewald, T. Döppner, et al., Design of a high-foot high-adiabat ICF capsule for the National Ignition Facility, Phys. Rev. Lett 112 (2014) 055002.
[7] O.A. Hurricane, D.A. Callahan, D.T. Casey, E.L. Dewald, T.R. Dittrich, et al., The high-foot implosion campaign on the National Ignition Facility, Phys. Plasmas 21 (2014) 056314.
[8] Z.F. Fan, S.P. Zhu, W.B. Pei, W.H. Ye, M. Li, et al., Numerical investigation on the stabilization of the deceleration phase Rayleigh-Taylor instability due to alpha particle heating in ignition target, EPL 99 (2012) 65003.
[9] R.M. More, K.H. Warren, D.A. Young, G.B. Zimmerman, A new quotidian equation of state (QEOS) for hot dense matter, Phys. Fluids 31 (1988) 3059.

[10] M.A. Vronskii, Yu. V. Koryakina, Electron-ion relaxation time in moderately degenerate plasma, Plasma Phys. Rep. 41 (9) (2015) 737−743.
[11] J.R. Rygg, J.A. Frenje, C.K. Li, F.H. Seguin, R.D. Petrasso, Electron-ion thermal equilibration after spherical shock collapse, Phys. Rev. E 80 (2009) 026403.
[12] G.S. Fraley, E.J. Linnebur, R.J. Mason, R.L. Mose, Thermonuclear burn characteristics of compressed deuterium-tritium microspheres, Phys. Fluids 17 (2) (1974) 474−489.
[13] The ion temperature is averaged by $T_i=\sigma v^{-1}(\int\rho^2\sigma v(T_i)r^2\mathrm{d}r\ /\int\rho^2r^2\mathrm{d}r\ )$, where σv is the DT reactivity; and the electron temperature is averaged by $T_e=(\int\rho^2T_e^{1/2}r^2\mathrm{d}r/\int\rho^2r^2\mathrm{d}r)^2$.
[14] T. Ma, P.K. Patel, N. Izumi, P.T. Springer, M.H. Key, et al., Onset of hydrodynamic mix in high-velocity, highly compressed inertial confinement fusion implosions, Phys. Rev. Lett. 111 (2013) 085004.
[15] V.Y. Glebov, T.C. Sangster, C. Stoeckl, J.P. Knauer, W. Theobald, et al., The National Ignition Facility neutron time-of-flight system and its initial performance, Rev. Sci. Instrum. 81 (2010) 10D325.
[16] D.L. Bleuel, C.B. Yeamans, L.A. Bernstein, R.M. Bionta, J.A. Caggiano, et al., Neutron activation diagnostics at the National Ignition Facility, Rev. Sci. Instrum. 83 (2012) 10D313.
[17] D.T. Casey, J.A. Frenje, M. Gatu Johnson, F.H. Séguin, C.K. Li, et al., Measuring the absolute deuterium-ctritium neutron yield using the magnetic recoil spectrometer at OMEGA and the NIF, Rev. Sci. Instrum. 83 (2012) 10D912.
[18] S. Glenn, J. Koch, D.K. Bradley, N. Izumi, P. Bell, et al., A hardened gated X-ray imaging diagnostic for inertial confinement fusion experiments at the National Ignition Facility, Rev. Sci. Instrum. 81 (2010) 10E539.
[19] T. Ma, N. Izumi, R. Tommasini, D.K. Bradley, P. Bell, et al., Imaging of high-energy X-ray emission from cryogenic thermonuclear fuel implosions on the NIF, Rev. Sci. Instrum. 83 (2012) 10E115.
[20] N. Izumi, T. Ma, M. Barrios, L.R. Benedetti, D. Callahan, et al., Measurement of electron temperature of imploded capsules at the National Ignition Facility, Rev. Sci. Instrum. 83 (2012) 10E121.
[21] D.H. Edgell, D.K. Bradley, E.J. Bond, S. Burns, D. A Callahan, et al., South pole bang-time diagnostic on the National Ignition Facility, Rev. Sci. Instrum. 83 (2012) 10E119.
[22] Z.F. Fan, X.T. He, J. Liu, G.L. Ren, B. Liu, et al., A wedged-peak-pulse design with medium fuel adiabat for indirect-drive fusion, Phys. Plasmas 21 (2014) 100705.